Endoscopic Ultrasound Spectrum Analysis for *In Vivo* Characterization of Pancreatic and Lymph Node Tissue: A Pilot Study

Ronald E. Kumon, PhD, Kayode Olowe, MD, Ashley L. Faulx, MD, Farees T. Farooq, MD, Victor K. Chen, MD, MSPH, Yun Zhou, MS, Richard C. K. Wong, MD, Gerard A. Isenberg, MD, Michael V. Sivak, MD, Amitabh Chak, MD, Cheri X. Deng, PhD

Current affiliations: Division of Gastroenterology, University Hospitals Case Medical Center and Case Western Reserve University, Cleveland, Ohio, USA (K.O., A.L.F., F.T.F., V.K.C., R.C.K.W., G.A.I., M.V.S., A.C.), Department of Biomedical Engineering, The University of Michigan, Ann Arbor, Michigan, USA (R.E.K., Y.Z., C.X.D.)

Participating Institutions: Division of Gastroenterology, University Hospitals Case Medical Center, Case Western Reserve University, Cleveland, Ohio, USA, and Department of Biomedical Engineering, Case Western Reserve University, Cleveland, Ohio, USA

Running title: In Vivo EUS Spectrum Analysis of Pancreas & Lymph Nodes

Meeting presentations: The results of this study will be presented at Digestive Disease Week, Washington DC, May 19 to 24, 2007 (Gastroenterology 2007, forthcoming).

Grant support: This work is supported in part by the Ohio Wright Center of Innovation/Biomedical Research and Technology Transfer Grant "Biomedical structural, functional and molecular imaging enterprise." Amitabh Chak is supported by a K24 Midcareer Award in Patient Oriented Research, National Institutes of Health (Grant DK002800).

Conflict of interest disclosures: None

Corresponding author and reprint requests: Amitabh Chak, Division of Gastroenterology, University Hospitals Case Medical Center, 11100 Euclid Ave., Cleveland, Ohio 44106–5066, USA, 216–844–5385 (business) 216–938–0347 (fax), amitabh.chak@case.edu

Author contributions: (A) Conception and design [A.L.F., A.C., C.X.D., R.E.K., F.T.F.]; (B) Analysis and interpretation of the data [R.E.K., V.K.C., K.O., F.T.F., Y.Z., R.C.K.W., G.A.I., M.V.S., A.C., C.X.D.]; (C) Drafting of the article [R.E.K., F.T.F.]; (D) Critical revision of the article for important intellectual content [all]; (E) Final approval of the article [all]

Abstract

Background: EUS is limited by variability in the examiner's subjective interpretation of B-scan images to differentiate between normal, inflammatory, and malignant tissue. By using information otherwise discarded by conventional EUS systems, quantitative spectral analysis of the raw radio-frequency (RF) signals underlying EUS images enables tissue to be characterized more objectively.

Objective: To determine the feasibility of using spectral analysis of EUS data for characterization of pancreatic tissue and lymph nodes.

Design & Setting: A pilot study of eligible patients was conducted to analyze the RF data obtained during EUS using spectral parameters.

Patients: Twenty-one subjects who underwent EUS of the esophagus, stomach, pancreas, and surrounding intra-abdominal and mediastinal lymph nodes.

Interventions: NA

Main Outcome Measurements: Linear regression parameters of calibrated power spectra of the RF signals were tested to differentiate normal pancreas from chronic pancreatitis and from pancreatic cancer, as well as benign from malignant-appearing lymph nodes.

Results: The mean intercept, slope, and mid-band fit of the spectra differed significantly among normal pancreas, adenocarcinoma, and chronic pancreatitis when all were compared to each other ($p < 0.01$). On direct comparison, mean mid-band fit for adenocarcinoma differed significantly from chronic pancreatitis ($p < 0.05$). For lymph nodes, mean mid-band fit and intercept differed significantly among benign- and malignant-appearing lymph nodes ($p < 0.01$ and $p < 0.05$, respectively).

Published in Gastrointestinal Endoscopy, Vol. 66, no. 6, pp. 1096–1106, 2007.

Limitations: Small sample population and spatial averaging inherent to this technique.

Conclusions: Mean spectral parameters in EUS imaging can provide a non-invasive method to discriminate normal from diseased pancreas and lymph nodes.

Keywords: Endoscopic ultrasound, Spectrum analysis, Ultrasound backscatter, Pancreatic cancer, Lymph nodes

INTRODUCTION AND BACKGROUND

Treatment algorithms and the mortality rates of GI cancers are primarily determined by the clinical stage at diagnosis, classified by depth of invasion, presence of regional lymph nodes, and presence of distant metastases.[1] The accuracy of various imaging modalities in the detection and staging of GI cancers, particularly pancreatic cancer, has been variable and at times disappointing. As early detection and accurate tumor staging have a clear clinical impact, technologies that can improve tumor detection, distinguish benign from malignant tissue, and identify the spread of cancer to lymph nodes are needed.

In most centers EUS has been adopted as the method of choice for the locoregional staging of esophageal, gastric, and rectal cancers, and to a lesser extent pancreatic cancer. However, the accuracy of EUS for these indications varies and is influenced by T stage, traversability of the tumor, and operator/center experience.[2-7] EUS imaging relies primarily on subjective operator judgements regarding changes in the B-scan grayscale sonographic characteristics of the imaged regions of interest (ROI). Imaging characteristics used to predict histologic diagnosis of a lesion typically include size, morphology, relative echogenicity, and level of homo- or heterogeneity. Deciphering these characteristics in real-time is contingent on the ability of the naked eye to detect grayscale nuances. The task is most difficult in the context of identifying pancreatic cancers in the setting of chronic pancreatitis[8] and differentiating benign from malignant lymph nodes.[9,10] An objective means of differentiating benign or inflammatory tissue processes from neoplastic or malignant processes could improve diagnostic capability of EUS and significantly impact patient care.

While grayscale B-mode EUS imaging can often identify tissue boundaries, it has limited ability to distinguish between tissue types. In contrast, tissue characterization based on spectrum analysis from the backscattered radio-frequency (RF) ultrasound signals has proven to be an effective technique for distinguishing malignant tumors from benign tumors and other pathologies in the context of ocular, prostate, and breast cancer,[11–13] for assessing diffuse and focal liver disease by trans-abdominal ultrasound,[14] for identifying atherosclerotic plaque via intravascular imaging,[15] and for assaying tissue changes induced by hyperthermia.[16] Ultrasound is backscattered due to locally inhomogeneous tissue or other acoustical scatterers. The backscatter characteristics depend on the effective size and concentration of the scatterers, as well as the acoustic impedance (density and sound speed) of the tissue. For example, a malignant tumor may scatter ultrasound differently than normal tissue because of its different microstructure. Analysis of the backscattered RF signals may therefore allow different tissue types to be distinguished.[17] The assessment by spectral parameters is quantitative and, with proper calibration, is independent of the system and user.

However, only limited work has been performed using ultrasound backscatter for characterization of GI cancer, particularly *in vivo*. Studies of lymph node metastases of colorectal cancer have shown that ultrasound backscatter analysis performed better than B-mode ultrasound[18] and that even consideration of multiple B-mode sonographic parameters may be insufficient for identifying metastases.[19] To our knowledge, ultrasound spectrum analysis has not been previously used in the arena of EUS.

In this "proof of principle" *in vivo* study, we investigate the use of spectral analysis of EUS backscattered signals to distinguish between (1) normal pancreas,

pancreatic cancer, and chronic pancreatitis, and (2) benign- and malignant-appearing intra-abdominal and mediastinal lymph nodes.

METHODS

Patients and clinical protocol

A total of 21 patients (8 men and 13 women; mean age 67, range 36–87) already scheduled for EGD/EUS were enrolled in this study. As the data acquisition process does not affect the procedure itself, a waiver of patient consent for this study was granted by our institutional review board. The indications for the procedures included suspected neoplasia of the esophagus (3 cases), stomach (5 cases), and pancreas (13 cases). In some cases images were also taken in areas outside of the organ of primary interest, to act as normal controls for various organs.

Data acquisition

A commercially available clinical ultrasound system (Model Exera EU-M60, Olympus America, Center Valley, Pa) was used with an ultrasonic gastrovideoscope (Model GF-UM160, Olympus America, Center Valley, Pa). The endoscope tip contains a light guide for obtaining video endoscopy images and a single-element transducer that spins about the axis of the scope in the lumen, thereby creating B-scan cross-sectional images, each one of which consists of a series of 256 consecutive A-scan lines. With assistance from Olympus America, a specially equipped output port of the ultrasound console allowed RF data access without affecting the normal operation of the system. The RF data were captured using a digital oscilloscope (Model LT372, LeCroy Corporation, Chestnut Ridge, NY) in 8-bit mode at sampling rates of either 100 or 200 million samples per second. In each case where RF data were acquired, the B-scan image generated by the

Olympus system (henceforth called "the system image") was also saved. The acquisition could not be achieved simultaneously due to technical limitations of the data transfer speed, but were taken as close together as possible, with a time delay less than a few seconds. In all the cases reported in this paper, data were acquired when the EUS system was operated in the C5 mode (transducer center frequency 6 MHz, transducer focal distance 20 mm, pulse repetition frequency 3.415 kHz). It was verified that the RF signals from the special output port were obtained prior to time-gain compensation or other processing used to generate the conventional B-mode image.

Data analysis

The RF data were imported into our custom-designed, MATLAB-based analysis software with a graphical user interface for image reconstruction and data processing (MATLAB 2006b, Mathworks, Natick, Mass). The B-scan image from the RF data was reconstructed and then oriented to match the system image using identifiable landmarks on the image. The orientation was used for convenience of comparison because the first A-scan acquisition from the RF data stream was arbitrary.

Prior to RF data analysis, regions of interest (ROIs) were identified and manually segmented by endosonographers on the system image according to the evaluation criteria described below. The ROIs were then independently translated onto the reconstructed image to select corresponding segments of RF data. Each sector-shaped area was sized to be as large as possible within the designated ROIs. The power spectrum was calculated for the signals of each A-scan RF data within the ROI gated by a series of sliding Hamming windows[20] of 1.5 μs each offset by 0.1 μs. The window length corresponded to approximately 2.3 mm in space.

To remove artifacts associated with the composite transfer function of the electronic transmitter/receiver and transducer, calibration was performed by dividing the power spectrum by the spectrum of a perfect reflector, in this case, simulated by a 38 mm diameter glass cylinder filled with water. Figure 1 shows the measured pulse and corresponding normalized power spectrum in dB. The spectrum is broad, fairly uniform, and generally consistent with the center frequency specified by the manufacturer.

As the calibrated spectra are typically quasi-linear in shape over the ultrasound frequency range used, a linear regression was performed to obtain slope and intercept along with the *mid-band fit*, the value of the linear function evaluated at the midpoint of the −15dB bandwidth. The square of the correlation coefficient R^2 for each fit was also recorded as a simple measure of the deviation of the calibrated spectrum from linearity.

B-mode evaluation

B-mode pancreas images were classified according to the following definitions: (1) *Chronic pancreatitis* was defined by the presence of greater than or equal to five of the following established EUS criteria:[22] (a) hyperechoic foci, (b) hyperechoic stranding, (c) lobularity, (d) cyst, (e) calcification, (f) ductal dilation, (g) side branch dilation, (h) duct irregularity, (i) hyperechoic duct margins, (j) atrophy, and (k) inhomogeneous echo pattern. (2) *Pancreatic cancer* was defined by the presence of a mass lesion identified by EUS with fine needle aspiration cytopathology, ERCP brush cytology, or subsequent surgical pathology consistent with adenocarcinoma. (3) *Normal pancreas* was defined by the presence of normal, homogeneous pancreatic echogenicity and the absence of mass lesions or any EUS features of chronic pancreatitis.

B-mode lymph nodes images were classified as benign or malignant according to the following definitions: (1) *Malignant lymph nodes* were defined as nodes seen in association with a GI tract mass lesion (*eg*, esophagus, stomach, pancreas) and having either a lymph node FNA cytolopathology consistent with adenocarcinoma or demonstrating greater than or equal to three established EUS features of malignant lymphadenopathy:[9,23] (a) diameter > 1cm, (b) round or oval shape, (c) diffusely hypoechoic, (d) sharp edges. (2) *Benign lymph nodes* were defined as nodes seen on EUS examination in the absence of GI tract mass lesions or known diagnosis of cancer, lacking EUS features of malignant nodes, and demonstrating at least 1 established criterion for benign lymph nodes: (a) draping configuration, (b) hyperechoic core, (c) diameter < 1 cm.

Statistical analysis

The spectral parameters generated from each window were averaged over each ROI. The resulting values were then analyzed using a one-way ANOVA for the three tissue types in the pancreas data, and Student's *t* test for the two tissue types in the lymph-node data. In some situations where the number of cases was small, the corresponding nonparametric statistics were also computed using the Wilcoxon rank sum test.[24] The statistical calculations were performed by routines from the MATLAB Statistical Toolbox (Version 2006b, Mathworks, Natick, Mass).

RESULTS

Pancreas

RF data from 16 subjects (10 women, 6 men; mean age 67; range 36–85) were examined, yielding a total of 32 ROIs in the resulting images. Figure 2 shows a

comparison of system images with the analysis images reconstructed from the RF data for selected cases of normal pancreatic body, adenocarcinoma, and chronic pancreatitis, along with typical calibrated spectra from those cases. Normal tissue included tissue from the uncinate, head, and body. The major features of the system image are clearly identifiable in the reconstructed image. Minor differences in appearance between the system and reconstructed images occur because no image processing (smoothing, contrast, etc.) for display purposes is applied in the reconstructed image and a slight movement between the acquisitions of the images could occur. The appearance of differences should not affect the results because the analysis was performed on the RF data directly and the system images were only for selection of ROIs.

The features of interest were manually segmented in the system images as shown in Figure 2. This segmentation was then manually translated onto the reconstructed image within which an ROI was selected. All ROIs had the sector shape shown in the images with the current version of the analysis software. Distinct differences can be seen between the spectra in each case.

A summary of the mean values over each ROI for each spectral parameter for all the examined regions is given in Table 1. The mid-band fit, intercept, and correlation coefficient were higher on average for normal cases than the adenocarcinoma and chronic pancreatitis, while the slope was lower (more negative) on average. ANOVA calculations (assuming equal variance between groups) were performed to test the null hypothesis that the mean values of each spectral parameter from each tissue type are equal, with the results listed in the last two rows of Table 1. In all cases, $p < 0.01$, indicating that at least one of the tissue types is distinguishable from the others. Figure 3 shows the

corresponding box plots of each tissue type for each spectral parameter. The figure shows that normal pancreas is well-distinguished from the pancreatic cancer and chronic pancreatitis for the mid-band fit, intercept, and correlation coefficient, but there is more overlap for the slope. Post hoc multiple comparisons performed using the Bonferroni criterion indicated that only normal pancreas could be distinguished from diseased pancreas at the $p = 0.05$ significance level.

While the differences between adenocarcinoma and chronic pancreatitis may not be considered significant by the Bonferroni criterion, the box plots of Figure 3 suggest that there are emerging trends. For example, a direct comparison of the mean values by Student's *t* test assuming unequal variance shows that even with the modest sample size ($N = 7$), the means of the mid-band fit are statistically different with $p = 0.048$. If the data are further analyzed using nonparametric analysis (Wilcoxon rank sum test), the medians of the mid-band fit, intercept, and correlation coefficient are close to being significantly different with $p = 0.057$.

Lymph nodes

RF data from 7 subjects (4 women, 3 men, mean age 65, range 52–79) were examined, yielding a total of 14 ROIs in the resulting images. Figure 4 shows a comparison of system images with the images reconstructed from the RF data for selected cases of benign and malignant lymph nodes, along with typical calibrated spectra from those cases. The spectra show distinguishable differences in all the spectral parameters.

Table 2 lists the mean and standard deviation of all the spectral parameters for the benign- and malignant-appearing lymph nodes along with results of applying Student's *t*

test assuming unequal variance to compare the means of the two groups. The benign-appearing nodes have higher mid-band fit, lower (more negative) slope, higher intercept, and higher correlation coefficient than the malignant-appearing nodes. The mid-band fit and intercept show statistically significant differences between the groups at the $p < 0.01$ and $p < 0.05$ levels, respectively. The same conclusion holds under a nonparametric analysis (Wilcoxon rank sum test).

DISCUSSION

B-mode imaging uses only the amplitude of the envelope of the B-mode RF data to produce the grayscale encoding in the image, ignoring the frequency and phase information of the signal that may include potentially useful information about tissue properties. The displayed image is also manipulated and subjected to many variables making quantitative comparisons and characterizations virtually impossible to implement. The primary advantage of the spectral analysis of RF signals over conventional B-mode imaging is that the spectral analysis permits objective and quantitative measurements of tissue properties by reducing the instrument-, setting-, and user-dependences inherent in grayscale B-mode interpretation. For example, the spectral parameters slope and intercept depend upon the size and concentration of scatterers.[17] The mid-band fit value increases as the scatter concentration increases and the slope increases as the scatterer size decreases down to a lower bound.[17] As the spectral analysis procedure uses information already available in existing EUS systems, clinical implementation could be done with minimal modification to current equipment and procedures. The procedure is also applicable to systems with digital signals and linear arrays.

One limitation of the method is that the spatial averaging inherent in the ROI method limits the spatial resolution over which the spectral parameters can be computed. The use of higher frequencies may improve this resolution, provided that the tissue to be imaged is close enough to the transducer so the signals are not decreased severely by attenuation. A small number of ROIs were analyzed from data taken in the C7.5 (9 MHz center frequency, 14.5 MHz usable bandwidth) and C12 (10 MHz center frequency, 16.8 MHz usable bandwidth) modes of the EUS system and in some cases it appeared that better discrimination between tissue types could be achieved. However, a more systematic study is needed to confirm this result.

The diagnosis of chronic pancreatitis in this study was defined using clinical and "classic" EUS criteria. It is noted that short of histology there is no clinical "gold standard" for diagnosing chronic pancreatitis. Therefore only well defined cases of normal pancreas, chronic pancreatitis, and pancreatic cancer and well defined malignant and benign lymph nodes were studied to reduce the uncertainty of diagnosis. This is a proof of principle study with the objective to illustrate the potential power of this method.

Additional work is necessary to fully demonstrate the effectiveness of the technique. Large scale prospective studies are required to determine the utility of this technique for diagnosing chronic pancreatitis and for differentiating chronic pancreatitis from pancreatic cancer. Similarly, large studies that include a spectrum of lymph nodes will be required to define the clinical utility of this technique for characterizing lymph nodes. By collecting additional *in vivo* data and then confirming diagnosis with histology of the imaged tissue from biopsy or resection, linear discriminant analysis or classification and regression trees (CART) analysis can be performed and receiver

operator characteristic (ROC) curves can be computed. Scatterplots of the current data (not shown) indicate that with additional data the use of multiple parameters will be useful for classification of tissue type. *Ex vivo* characterization of resected tissue may also be helpful to obtain a more thorough understanding of the relationship between the measured spectral parameters and the physical and histological characteristics of the tissue. Ideally, a classification scheme could be developed that would allow for real time parametric images, in which grayscale B-mode images could be encoded or "digitally stained" with coloration corresponding to the probability of various normal or disease states, during the clinical examination itself. The development of such real time spectral analysis could lead to improved targeting of pancreatic lesions and lymph nodes for EUS guided fine needle aspiration.

CONCLUSION

This study examined the hypothesis that spectral parameters computed from EUS RF backscatter from *in vivo* examinations of the pancreas and intra-abdominal and mediastinal lymph nodes can differentiate the pathologies. The results suggest that individual mean spectral parameters such as mid-band fit and intercept can provide a method to discriminate between normal pancreas and diseased pancreas, benign-appearing and malignant-appearing lymph nodes, and possibly between adenocarcinoma and chronic pancreatitis. Additional work is needed to expand these encouraging results.

ACKNOWLEDGMENTS

The authors would like to acknowledge Olympus for making the RF data available and Brian Wolf for his technical assistance with the EUS system.

CAPSULE SUMMARY

What is already known on this topic

- Identifying pancreatic cancers in the setting of chronic pancreatitis and differentiating benign from malignant lymph nodes can be challenging using conventional grayscale EUS imaging.
- Spectral analysis of ultrasound backscatter has been previously demonstrated in non-EUS contexts to be an objective, quantitative method for tissue characterization and uses information in the backscattered ultrasound signals otherwise discarded in grayscale EUS imaging.

What this study adds to our knowledge

- This pilot study shows that spectral parameters such as mid-band fit and intercept of the EUS backscatter spectra can quantitatively discriminate between normal pancreas and diseased pancreas, benign-appearing and malignant-appearing lymph nodes, and possibly between adenocarcinoma and chronic pancreatitis.

REFERENCES

1. AJCC Cancer Staging Manual. 5th ed. Philadelphia, Pa: Lippincott-Raven; 1997. p. 65–68.
2. Van Vliet EP, Eijkemans MJ, Poley JW, Steyerberg EW, Kuipers EJ, Siersema PD. Staging of esophageal carcinoma in a low volume EUS center compared with reported results from high volume centers. Gastrointest Endosc 2006;63:938–947.
3. Willis S, Truong S, Gribnitz S, Fass J, Schumpelick V. Endoscopic ultrasonography in the preoperative staging of gastric cancer: Accuracy and impact on surgical therapy. Surg Endosc 2000;14:951–4.
4. Botet JF, Lightdale CJ, Zauber AG, Gerdes H, Winawer SJ, Urmacher C, et al. Preoperative staging of gastric cancer: Comparison of endoscopic US and dynamic CT. Radiology 1991;181:426–32.
5. Meyenberger C, Huch Boni RA, Bertschinger P, Zala GF, Klotz HP, Krestin GP. Endoscopic ultrasound and endorectal magnetic resonance imaging: a prospective, comparative study for preoperative staging and follow-up of rectal cancer. Endoscopy 1995;27:469–79.
6. Rifkin MD, Ehrlich SM, Marks G. Staging of rectal carcinoma: Prospective comparison of endorectal US and CT. Radiology 1989;170:319–22.
7. Dewitt J, Devereaux BM, Lehman GA, Sherman S, Imperiale TF. Comparison of endoscopic ultrasound and computed tomography for the preoperative evaluation of pancreatic cancer: A systematic review. Clin Gastroenterol Hepatol 2006;4:717–25.
8. Bhutani MS, Gress FG, Giovannini M, Erickson RA, Catalano MF, Chak A, et al. The No Endosonographic Detection of Tumor (NEST) study: A case series of

pancreatic cancers missed on endoscopic ultrasonography. Endoscopy 2004 May;36(5):385–389.

9. Catalano MF, Alcocer E, Chak A, Nguyen CC, Raijman I, Geenan JE, et al. Evaluation of metastatic celiac axis lymph nodes in patients with esophageal carcinoma: accuracy of EUS. Gastrointest Endosc 1999 Sep;50(3):352–356.
10. Kanamori A, Hirooka Y, Itoh A, Hashimoto S, Kawashima H, Hara K, et al. Usefulness of contrast-enhanced endoscopic ultrasonography in the differentiation between malignant and benign lymphadenopathy. Am J Gastroenterol 2006 Jan;101(1):45–51.
11. Lizzi FL, Greenebaum M, Feleppa EJ, Elbaum M, Coleman DJ. Theoretical framework for spectrum analysis in ultrasonic tissue characterization. J Acoust Soc Am 1983;73:1366–1373.
12. Tateishi T, Machi J, Feleppa EJ, Oishi R, Jucha J, Yanagihara E, et al. In vitro diagnosis of axillary lymph node metastatses in breast cancer by spectrum analysis of radio frequency echo signals. Ultrasound Med Biol 1998;24:1151–1159.
13. Lizzi FL, Feleppa EJ, Alam SK, Deng CX. Ultrasonic spectrum analysis for tissue evaluation. Pattern Recog Lett 2003;24:637–658.
14. King DL, Lizzi FL, Feleppa EJ, Wai PM, Yaremko MM, Rorke MC, et al. Focal and diffuse liver disease studied by quantitiative microstrutural sonography. Radiology 1985;155:457–462.
15. Nair A, Kuban BD, Obuchowski N, Vince DG. Assessing spectral algorithms to predict atherosclerotic plaque composition with normalized and raw intravascular ultrasound data. Ultrasound Med Biol 2001;27(10):1319–1331.

16. Lizzi FL, Astor M, Liu T, Deng C, Coleman DJ, Silverman RH. Ultrasonic spectrum analysis for tissue assays and therapy evaluation. Int J Imaging Sys Tech 1997;8:3–10.
17. Lizzi FL, Ostromogilsky M, Feleppa EJ, Rorke MC, Yaremko MM. Relationship of ultrasonic spectral parameters to features of tissue microstructure. IEEE Trans Ultrasonics Ferroelec Freq Control 1986;33:319–329.
18. Noritomi T, Machi J, Feleppa EJ, Yanagihara E, Shirouzu K. In vitro investigation of lymph node metastasis of colorectal cancer using ultrasonic spectral parameters. Ultrasound Med Biol 1998;24:235–243.
19. Tateishi T, Machi J, Feleppa EJ, Oishi AJ, Furumoto NL, Oishi RH, et al. In vitro investigation of detectibility of colorectal lymph nodes and diagnosis of lymph node metastasis in colorectal cancer using B-mode sonography. J Clin Ultrasound 2004;32:1–7.
20. Stremler FG. Introduction to Communication Systems. 3rd ed. New York, NY: Addison-Wesley; 1992.
21. Press WH, Flannery BP, Teukolsky SA, Vetterling WT. Numerical recipes in FORTRAN: The art of scientific computing. 2nd ed. New York, NY: Cambridge University Press; 1992.
22. Wallace MB, Hawes RH. Endoscopic ultrasound in the evaluation and treatment of chronic pancreatitis. Pancreas 2001 Jul;23(1):26–35.
23. Schmulewitz N, Wildi SM, Varadarajulu S, Roberts S, Hawes RH, Hoffman BJ, et al. Accuracy of EUS criteria and primary tumor site for identification of mediastinal lymph node metastasis from non-small-cell lung cancer. Gastrointest Endosc 2004;59:205–11.

24. Walpole RE, Myers RH, Myers SL, Ye K. Probability & Statistics for Engineers & Scientists. 8th ed. Upper Saddle River, NJ: Pearson Prentice Hall; 2007.

TABLE CAPTIONS

1. Means and standard deviations of spectral parameters from regions identified to be normal pancreas, pancreatic cancer, and chronic pancreatitis in the B-mode images. The table also lists the results of ANOVA calculations assuming equal variance between groups. In each case, there are 2 degrees of freedom for variance between groups and 29 degrees of freedom for variance within groups.
2. Means and standard deviations of spectral parameters from regions judged to be benign and malignant lymph nodes in the B-mode images. The table also lists the results of Student's *t* test under the assumption of unequal variances between the two groups, where the estimated number of degrees of freedom in each case is given by Satterthwaite's approximation.

Table 1

B-mode appearance	Mid-band Fit [dB]	Slope [dB/MHz]	Intercept [dB]	Correlation coeff. R^2
Normal (N = 25)	−23.4±3.2	−2.03±0.84	−11.0±5.4	0.41±0.11
Adenocarcinoma (N = 3)	−35.4±1.6	−0.76±0.67	−30.9±5.7	0.12±0.07
Chronic pancreatitis (N = 4)	−32.1±1.0	−1.08±0.18	−25.6±1.2	0.22±0.04
F-statistic	33.6	5.46	30.3	15.2
p-value	<0.001	<0.01	<0.001	<0.001

Table 2

B-mode appearance	Mid-band Fit [dB]	Slope [dB/MHz]	Intercept [dB]	Correlation coeff. R^2
Benign (N=8)	−26.7±4.3	−1.56±0.84	−17.3±4.3	0.28±0.11
Malignant (N=6)	−34.6±3.7	−1.18±0.81	−26.9±8.0	0.19±0.12
Est. degrees of freedom	11.7	11.1	7.2	11.6
T-statistic	−3.46	0.84	−2.67	−1.66
p-value	<0.01	0.42	<0.05	0.12

FIGURE CAPTIONS

1. **A,** Calibration pulse for the C5 mode. **B,** corresponding power spectrum. The usable bandwidth, defined by the −15 dB points is 8.5 MHz.
2. Example images and calibrated spectra: **A**–**C,** normal pancreas. **D**–**F,** adenocarcinoma. **G**–**I**, chronic pancreatitis. Images **A**, **D**, **G** were generated by the Olympus system (tic marks occur at 5 mm intervals on both axes). The segmentation was added manually after image acquisition. Images **B**, **E**, **H** were reconstructed from the RF data. The segmentation was transferred from the system images to the reconstructed images, and then the sector-shaped region of interest for the spectral analysis was selected inside the segmented area. Graphs **C**, **F**, **I** show selected average calibrated spectrum from within each ROI. (The dark region at the bottom of Image **E** appears because data were only acquired out to about 38.5 mm in range for this data set.)
3. Boxplots of the spectral parameters from the pancreas EUS data: **A,** mid-band fit. **B,** slope. **C,** intercept. **D,** correlation coefficient R^2. The boxes indicate the lower quartile, median and upper quartile values, while the whiskers show the extent of the rest of the data. The notches represent a robust estimate of the uncertainty about the medians for box-to-box comparison. Boxes whose notches do not overlap indicate that the medians of the two groups differ at the $p = 0.05$ significance level.
4. Example images and calibrated spectra: **A**–**C,** benign-appearing lymph nodes and **D**–**F,** malignant-appearing lymph nodes. Images **A** and **D** were generated by the Olympus system (tic marks occur at 5 mm intervals on both axes). The segmentation was added manually after image acquisition. Images **B** and **E** were reconstructed

from the RF data. The segmentation was transferred from the system images to the reconstructed images, and then the sector-shaped region of interest for the spectral analysis was selected inside the segmented area. Graphs **C** and **F** show selected average calibrated spectrum from within each ROI.

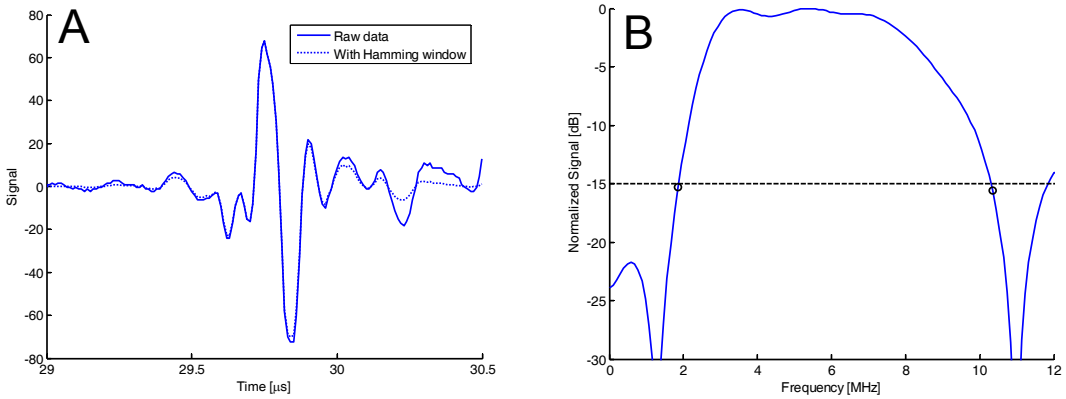
A
Raw data
With Hamming window
Signal
Time [μs]
B
Normalized Signal [dB]
Frequency [MHz]

Figure 1

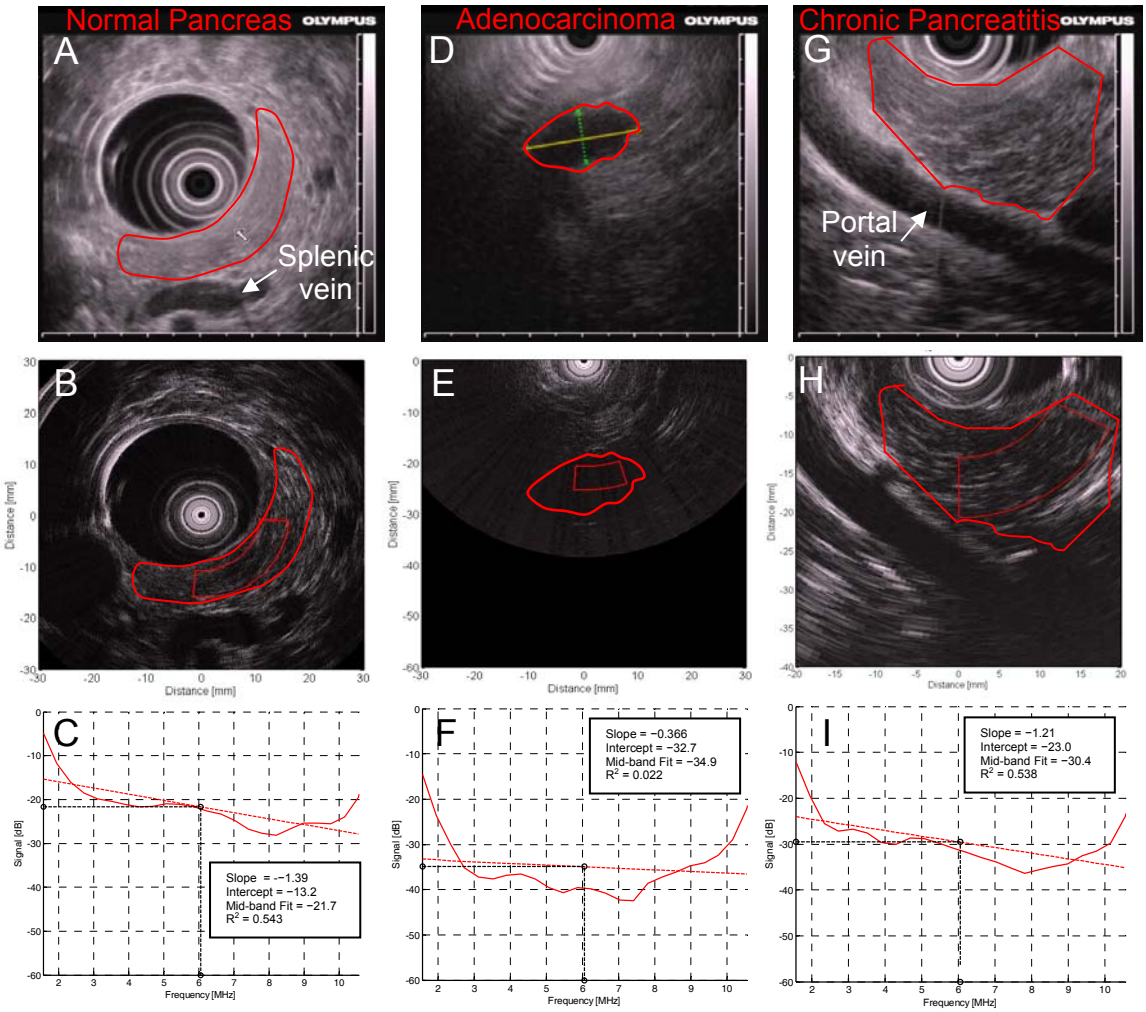
Normal Pancreas
OLYMPUS
A
Splenic vein
Adenocarcinoma
OLYMPUS
D
Chronic Pancreatitis
OLYMPUS
G
Portal vein
B
E
H
Distance [mm]
C
F
I
Signal [dB]
Frequency [MHz]
Slope = −1.39
Intercept = −13.2
Mid-band Fit = −21.7
R² = 0.543
Slope = −0.366
Intercept = −32.7
Mid-band Fit = −34.9
R² = 0.022
Slope = −1.21
Intercept = −23.0
Mid-band Fit = −30.4
R² = 0.538

Figure 2

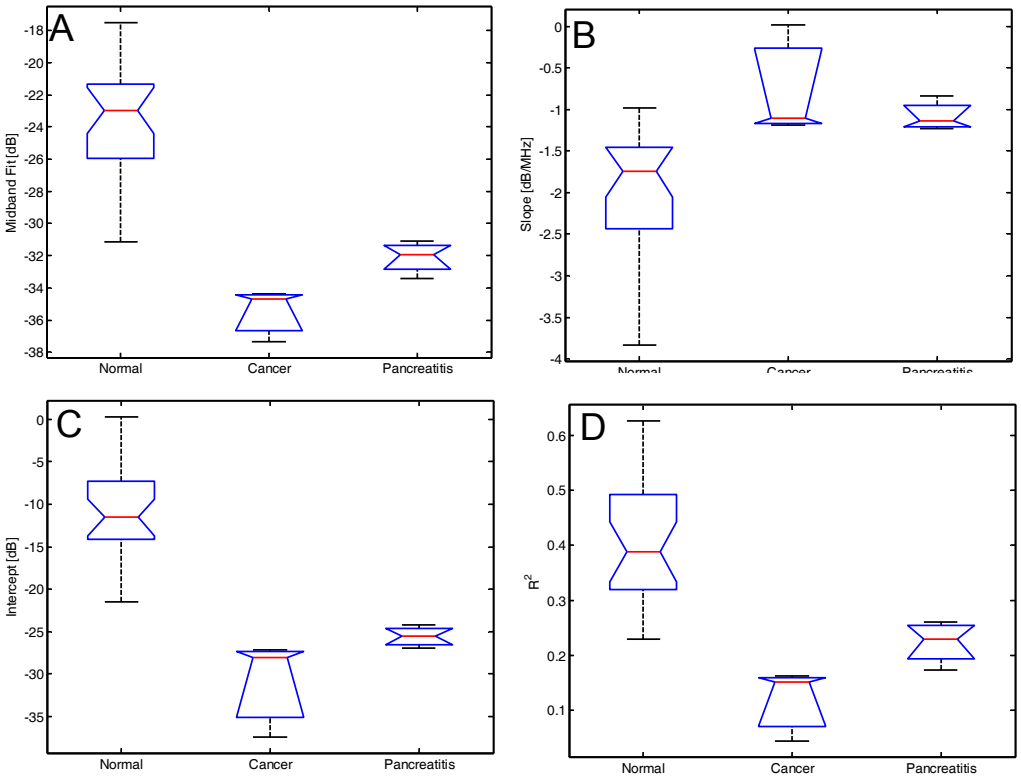
A
Midband Fit [dB]
-18
-20
-22
-24
-26
-28
-30
-32
-34
-36
-38
Normal
Cancer
Pancreatitis
B
Slope [dB/MHz]
0
-0.5
-1
-1.5
-2
-2.5
-3
-3.5
-4
C
Intercept [dB]
0
-5
-10
-15
-20
-25
-30
-35
D
R2
0.6
0.5
0.4
0.3
0.2
0.1

Figure 3

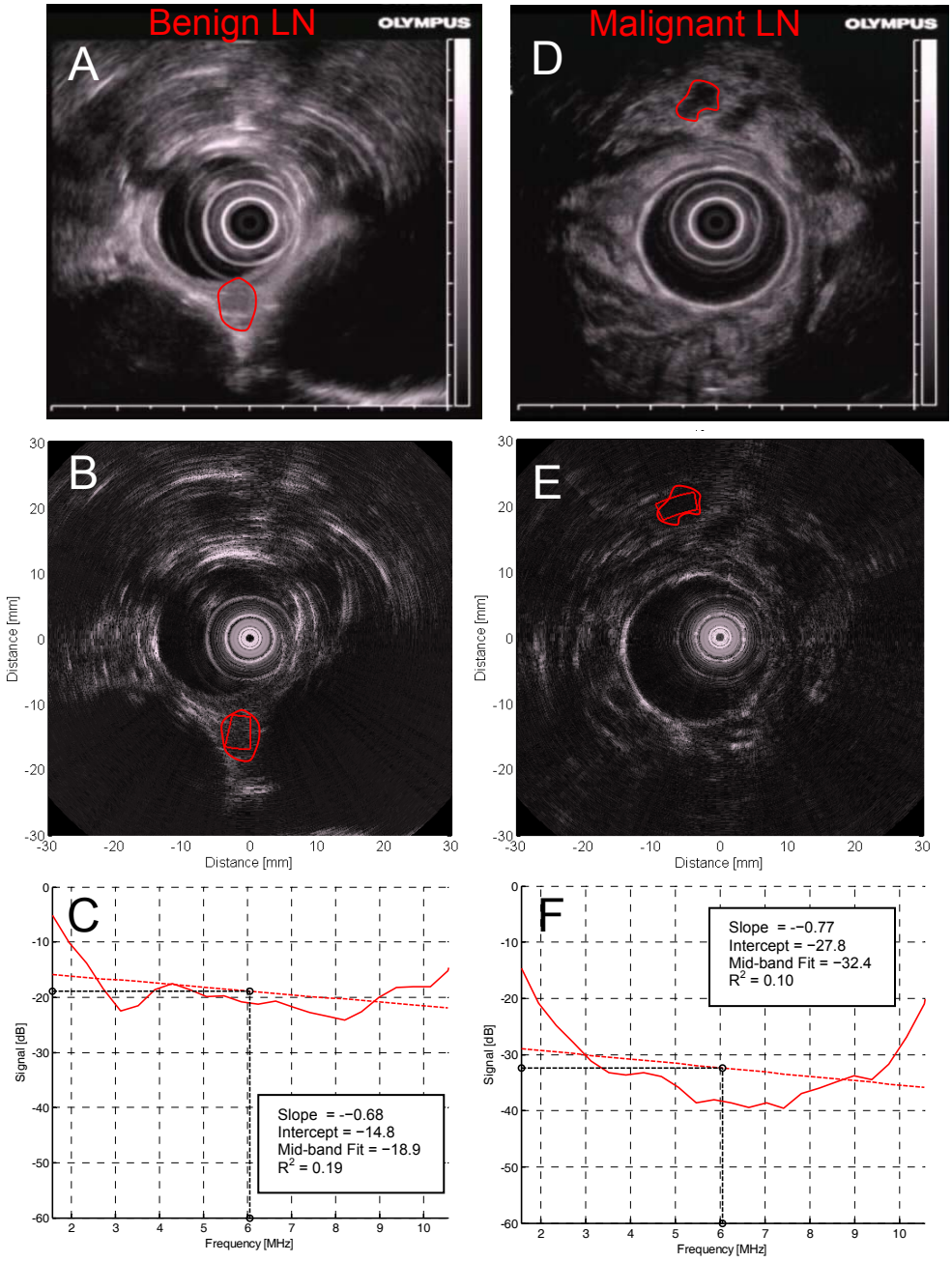
Benign LN
OLYMPUS
A
Malignant LN
OLYMPUS
D
B
E
Distance [mm]
Distance [mm]
Distance [mm]
C
Slope = -−0.68
Intercept = −14.8
Mid-band Fit = −18.9
R2 = 0.19
Signal [dB]
Frequency [MHz]
F
Slope = -−0.77
Intercept = −27.8
Mid-band Fit = −32.4
R2 = 0.10
Signal [dB]
Frequency [MHz]

Figure 4